J Nanopart Res (2023) 25:122
https://doi.org/10.1007/s11051-023-05769-4

RESEARCH PAPER

In situ electron microscopy techniques for nanoparticle dispersion analysis of commercial sunscreen

M. Ilett · E. Naveed · T. Roncal-Herrero · Z. Aslam · S. Micklethwaite · N. Hondow

Received: 8 March 2023 / Accepted: 17 May 2023 / Published online: 6 June 2023

Abstract Nanoparticles are common active ingredients within many commercial products including sunscreen. Consequently, accurate characterisation of nanoparticles in these products is vital to enhance product design, whilst also understanding the toxicological implications of these nanoparticles. Whilst bulk techniques are useful in providing some information, they often cannot resolve individual particles, and therefore electron microscopy can be used for high-resolution nanoparticle characterisation. However, conventional high vacuum dry TEM does not accurately represent nanoparticle dispersions and other in situ methods must be used. Here, we use a combination of techniques including liquid cell transmission electron microscopy (LCTEM), cryogenic (cryo)-TEM and cryo-scanning electron microscopy (SEM) to characterise a commercial sunscreen containing titanium dioxide (TiO_2) and zinc oxide (ZnO) nanoparticles. Our work illustrates that whilst LCTEM does not require any sample preparation more beam artefacts can occur causing ZnO dissolution with only TiO_2 nanoparticles visualised. Comparatively, cryo-TEM allows characterisation of both ZnO and TiO_2, yet only cryo-SEM could be used to analyse the pure product (without dilution) but biased the characterisation to the larger fraction of nanoparticles and agglomerates. Ultimately, only with a combination of different in situ EM techniques can an accurate characterisation of commercial products be achieved in order to ensure effective and safe product design and manufacture.

Keywords Nanoparticle dispersion · In situ TEM · STEM · Sunscreen · Titanium dioxide · Zinc oxide

Introduction

The use of nanomaterials in a range of cosmetic products has become increasingly common. Specifically, metal oxide nanoparticles (e.g. zinc oxide and titania) are often an active ingredient in sunscreens. This is due to their intrinsic UV absorbing properties making them powerful physical UV blockers [1]. The use of nanoscale particles can greatly aid aesthetic benefits as smaller particles absorb visible wavelengths ensuring the product is transparent on the skin. However, there are indications that the nanoparticle size can also effect the UV blocking performance of a sunscreen, where in the case of TiO_2 nano-size can alter the mechanism of UV attenuation and also the wavelength at which greatest attenuation occurs [2, 3]. Furthermore, studies that look at assessing the potential toxicity of sunscreens have also linked the size and consequently the dispersion of the nanoparticles on the skin with potential

Supplementary Information The online version contains supplementary material available at https://doi.org/10.1007/s11051-023-05769-4.

M. Ilett (✉) · E. Naveed · T. Roncal-Herrero · Z. Aslam · S. Micklethwaite · N. Hondow
School of Chemical and Process Engineering, University of Leeds, Leeds LS2 9JT, UK
e-mail: m.a.ilett@leeds.ac.uk

toxicity, where typically smaller nanoparticles give rise to higher toxicity [4–6]. Therefore, accurate characterisation of the physiochemical properties of the active ingredients within these sunscreens including nanoparticle size, morphology and dispersion is essential to guarantee the highest quality product is produced both in terms of functionality and safety.

Traditionally, nanoparticle dispersions have been characterised using a range of bulk techniques, including, UV–visible absorption, X-ray diffraction (XRD) and dynamic light scattering (DLS). For the analysis of sunscreens, UV–visible spectroscopy quickly and simply assesses UV blocking capabilities. XRD is used to identify the structure of crystalline components, important as some of these have been shown to influence nanotoxicity [7]. However bulk techniques such as DLS which measures size distribution can be limited for more complex dispersions, where signals cannot be assigned to a specific nanoparticle or distinguished from other components inherent in the sunscreen [8]. Furthermore, it only provides a hydrodynamic radius measurement, no shape information can be obtained from these bulk measurements and yet shape is known to alter the biological behaviour of nanoparticles [9, 10]. An alternative to bulk characterisation is using electron microscopy (EM) which allows nanoscale resolution imaging alongside elemental analysis through, for example, energy-dispersive X-ray (EDX) spectroscopy. However, standard EM approaches necessitate a sample being completely dry due to the high vacuum requirements. For liquid samples such as nanoparticle dispersions this prevents characterisation of a product in its native hydrated state. The native hydrated state refers to the sample as it is in suspension, when samples are dried in air it is known that drying artefacts can occur which drive the rearrangement of nanoparticles on a TEM grid through the so called coffee ring effect [11]. Hence, this dried sample is no longer representative of the dispersion of nanoparticles in suspension [12]. Such limitations of conventional EM have led to the development and use of both cryogenic (cryo) and liquid cell (LC) EM. These in situ techniques allow characterisation of hydrated samples despite the high vacuum environment of the electron microscope.

Our previous work has shown that cryo-analytical-STEM is a powerful technique for characterisation of aqueous nanoparticle dispersions [13]. Yet, the development of LCTEM has allowed characterisation of an aqueous dispersion with no sample preparation at all. Such direct imaging of hydrated samples is clearly advantageous, however as research using this technique has increased it has become apparent that the electron beam can cause complicated changes in the chemistry of a sample, leading in some cases to beam induced artefacts [14]. One of the primary modes of beam interaction is through the radiolysis of the surrounding medium, commonly water [15]. We previously inferred that the lower temperatures in cryo-TEM would delay some of these beam induced artefacts due to the lower temperatures reducing at least some rates of reactions involved in radiolysis [16, 17]. In addition a reduction in the diffusion of damage products in solid vitreous ice compared to liquid water could also reduce beam induced damage [18]. In our previous work, we have shown that these differences do occur and can impact the study of crystallisation processes [19].

Typically, LCTEM is carried out using dedicated liquid cell holders, these allow a liquid to be sandwiched between two silicon nitride membrane windows. These dedicated holders are often equipped to flow liquid through the sample window as well as engineered to allow temperature control. However, this results in a complex piece of equipment, which are expensive, often costing upwards of £150,000 and require skilled users. A simpler and more cost-effective alternative is a static liquid cell. An example of this is through Bio-Matek who have designed a commercially available disposable static liquid cell ("K-kit") [20] able to fit in any standard TEM holder, and with a cost of ~£100 per cell and a start-up cost of £450 for the tool kit for assembly. It works on the same premise as a dedicated holder with a sample of liquid captured between two silicon nitride membrane windows; however, no liquid can be flowed through. This prevents the investigation of dynamic processes, but still allows important dispersion analysis to be carried out. Lu et al. [21] utilised the K-kit in order to characterise TiO_2 and ZnO nanoparticles in 3 commercial sunscreen sprays indicating the potential of these more simplistic liquid cell holders in providing in situ nanoparticle dispersion analysis. Further studies have also shown the benefits of using the K-kit in order to allow native state imaging of hydrated biological samples [22], including a study of nanoparticles within blood plasma [23].

In this work, we have utilised a model nanoparticle system [13] comprising of four known nanoparticles to investigate any differences in beam-sample interactions when characterising a nanoparticle dispersion through either cryo-TEM or LCTEM using the above described K-Kits. Following this, we provide a full characterisation of a commercial sunscreen containing ZnO and TiO_2 nanoparticles using both bulk and in situ EM techniques and show that there are discernible differences in measured nanoparticle agglomerate sizes identified through SEM and TEM, as well as electron beam induced artefacts occurring more readily during LCTEM analysis. Ultimately, we outline the advantages and limitations of both cryo-S/TEM and LCTEM and recommend where possible a combination of bulk and EM techniques are employed when characterising more complex nanoparticle dispersions.

Materials and methods

Nanoparticle dispersions

A model nanoparticle system used to investigate the scope of in situ EM techniques (previously reported in [13]) comprised of four nanoparticles dispersed in water; 50 µg/mL iron(III) oxide (primary particle size 40 nm; Fluka Chemika, Lot 40,095/1 22/00), 100 µg/mL cerium dioxide (primary particle size 10 nm; Joint Research Centre, NM-211), 50 µg/mL zinc oxide (primary particle size 20–60 nm; Nanotek, ZH1 121 W) and 20 µg/mL gold-silver core–shell nanoparticles (primary particle size 20 nm; Sigma-Aldrich; Lot# MKB19138V).

A commercial sunscreen (Simply Protect Kids Sunscreen SPF 50+, Banana Boat) was used for real product characterisation containing active ingredients of 4.5% of TiO_2 and 6.5% of ZnO and in-active ingredients of water, caprylic/capric triglyceride, isohexadecane, butyloctyl salicylate, octyldodecyl citrate crosspolymer, cetyl $PEG/PPG_{-10/1}$ dimethicone, lauryl PEG_{-8} dimethicone, C_{30}-C_{38} olefin/isopropyl maleate/MA copolymer, sodium chloride, ethylhexyl methoxycrylene, dimethicone, phenoxyethanol, caprylyl glycol, PEG_{-8}, alumina, glycerin, sodium citrate and tocopheryl acetate.

Cryogenic sample preparation

All samples were prepared for cryo-TEM using an FEI Mark IV Vitrobot©. A 3.5 µl drop of suspension was loaded onto a lacey carbon-coated copper TEM grid (EM resolutions) before being blotted and then rapidly plunge frozen in liquid ethane. Transfer into the microscope was done using a Gatan-914 cryo TEM holder, and the temperature was maintained below − 165 °C during analysis.

Samples were prepared for cryo-SEM using a Quorum Technologies PP3010 Cryo-SEM preparation system. The sunscreen sample was prepared by two methods: in its original state, and a sample "in use" where it was placed between two glass slides and systematically mixed to create a shearing process for approximately 10 min to imitate the procedure of rubbing the sunscreen on skin. In both cases, it was placed onto a copper rivet that was then plunged into slushed nitrogen (cooled to approximately − 210 °C). This was then transferred to the preparation chamber, pumped to 10^{-7} bar and cooled to − 140 °C. The sample was fractured with a cold knife and coated with iridium.

Static liquid cell preparation

A static liquid cell commercially sold as a K-kit and supplied by Bio-Matek was used [24]. These are single-use cells with a micro channel (2000 or 200 nm) between two silicon nitride membranes (30 nm), forming a central window for LCTEM (Fig. S1 in SI). The micro channel was filled with the sample via capillary action for 1 min before gluing the ends of the channel and mounting the whole cell on a specially designed copper grid. The glue was left to set under vacuum for 1 h and the assembled K-kit could then be loaded into any standard TEM holder.

In situ analytical EM

All S/TEM analysis was carried out using an FEI $Titan^3$ Themis G2 equipped with a monochromator operating at 300 kV and fitted with 4 EDX silicon drift detectors and a Gatan One-View CMOS camera. The probe current was kept below 100 pA for all cryo and LC experiments.

For cryo-SEM, an FEI Helios G4 CX Dual beam FIB-SEM was used with a beam voltage of 1–10 kV and beam current 100 pA, elemental mapping via EDX spectroscopy was conducted at 15 kV.

Bulk analysis

Extensive characterisation of the commercial sunscreen was carried out using a range of bulk techniques, including DLS, XRD and UV–visible spectroscopy. Further details of these procedures are found in the supplementary information.

Results and discussion

Liquid cell EM of model nanoparticle suspension

In order to examine the possibilities of using single use static liquid cells for characterising nanoparticle suspensions, a model nanoparticle dispersion was loaded into a K-kit and using STEM imaging and EDX mapping we could accurately identify and spatially locate the position of three of the nanoparticles within the dispersion, namely cerium oxide, iron oxide and zinc oxide (Fig. 1a–f). In our previous work [13], we characterised the same model nanoparticle suspension using cryo-S/TEM. Qualitative comparisons to this prior characterisation indicated the dispersion of the nanoparticles in the model suspension was the same in both the frozen and liquid samples, suggesting that both techniques provide valid approaches to dispersion analysis. However, there was evidence of nanoparticle dissolution within the liquid cell during electron beam irradiation, most significantly of

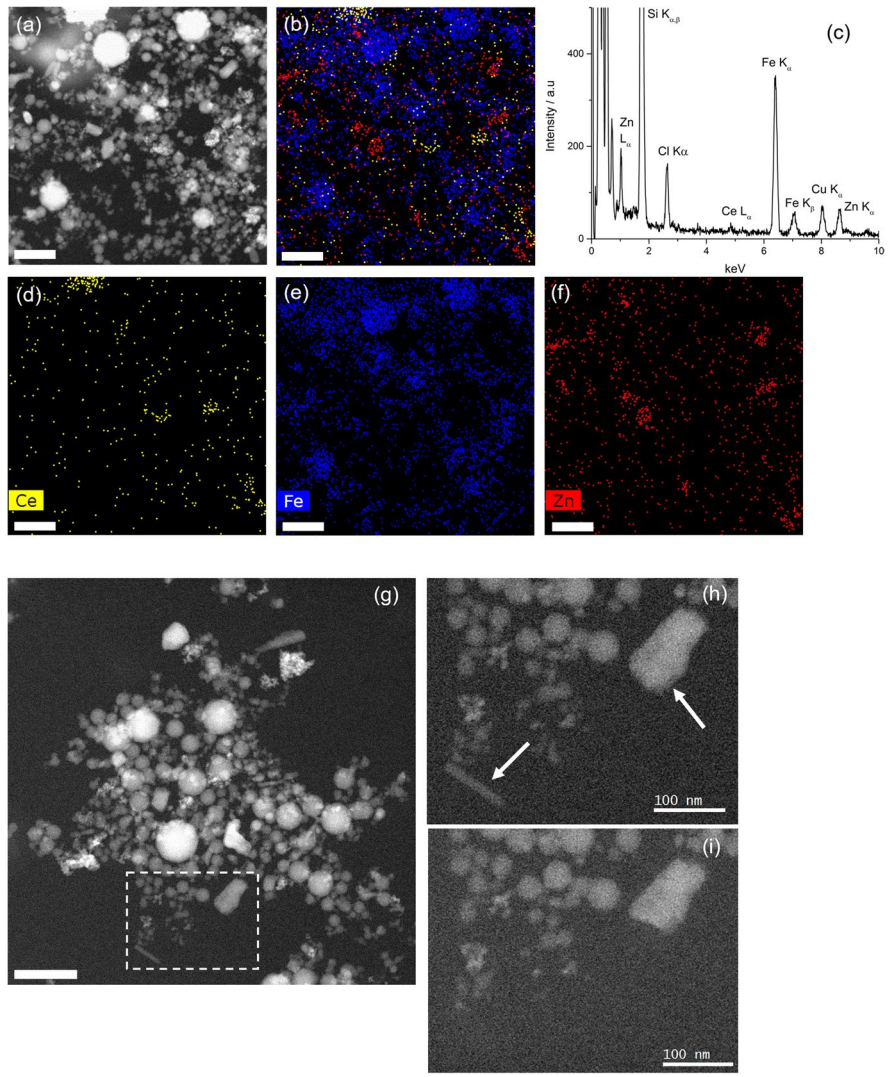

Fig. 1 STEM-EDX of a model nanoparticle suspension containing ZnO, Fe_2O_3, CeO_2 and Au–Ag core–shell nanoparticles, in a static liquid cell. (**a**) A HAADF STEM image of the model nanoparticle suspension from which the corresponding EDX maps and spectrum were obtained. From the EDX spectrum (**c**) mapping of Ce L_α (**d**), Fe K_α (**e**) and Zn L_α (**f**) X-rays is shown and a combined elemental map provided in (**b**). Total electron fluence was 300 $e^-/Å^2$. Evidence of nanoparticle dissolution in the static liquid cell was observed (**g**–**i**). An initial HAADF STEM image of the nanoparticle suspension in liquid was taken after exposure to an initial electron fluence of 30 $e^-/Å^2$ (**g**). Image (**h**) is the dashed region in (**g**) and (**i**) the same area after exposure to a further 300 $e^-/Å^2$. Clear dissolution of particles was observed and indicated by the white arrows in (**h**). (**a**–**g**) Scale bars are 200 nm

the ZnO nanoparticles (Fig. 1g–i). This dissolution is driven by electron beam interactions with the water, where beam induced water radiolysis causes the formation of H_3O^+ forcing a decrease in the pH [15, 25]. Since the solubility of ZnO increases in acidic environments [26], this explains the observed dissolution of ZnO. Such beam-induced dissolution was not previously observed during cryo-STEM analysis even at higher electron fluences, illustrating the potential benefit of cryo-EM over LCTEM in preventing or at least delaying some beam-induced artefacts. The lower temperatures in cryo-EM will reduce the rate of any reactions involved in water radiolysis [16, 17] and there will be significantly lower diffusion rates of damage products in vitreous ice compared to liquid water.

Application of in situ *electron microscopy to characterise commercial sunscreen*

A commercial sunscreen containing 4.5% TiO_2 and 6.5% ZnO was extensively characterised using traditional bulk techniques and in situ EM techniques. From bulk techniques, absorption in the UV–visible spectrum in the 280–400 nm range indicated the UV blocking functionality of the product (Fig. S2 in SI) and XRD confirmed the active ingredients of TiO_2 and ZnO (Fig. S3 in SI). An indication of the dispersion of the active ingredients from DLS analysis suggested the particles were agglomerated to some extent, with a Z average of 192 ± 86 nm (Fig. S4 in SI) compared to primary particle sizes of 81 ± 11 nm and 71 ± 32 nm for TiO_2 and ZnO nanoparticles respectively, obtained from TEM analysis of a dried sample (Fig. S5 in SI).

For in situ TEM characterisation, initial difficulties in loading the more viscous oil-based sunscreen into the liquid cell via capillary action were only overcome by diluting the product in water. This therefore prevented imaging and analysis of the product in a totally unmodified state. Upon loading, the diluted sunscreen into a K-kit we located and characterised the TiO_2 nanoparticles within the sample (Fig. 2a–c). These nanoparticles tended to exist as small agglomerates in agreement with the data from DLS. However, no ZnO nanoparticles were observed, most likely due to beam induced dissolution as was previously seen for the model nanoparticle suspension. Why the ZnO nanoparticles were not observed at all here compared to the model suspension where ZnO was observed initially before full dissolution under the electron beam could be explained by differences in particle size. The ZnO in the commercial sunscreen is smaller (~ 70 nm) as compared to the model suspension (> 100 nm) and smaller particles would be expected to dissolve more quickly. In addition, the ZnO nanoparticles in the model suspension have an aliphatic coating around them which has been previously shown to retard dissolution in certain media [27]. This therefore may slow some of the beam-induced dissolution, allowing them to be observed in the first instance in the model suspension.

Further beam interactions were observed from the beam induced movement of TiO_2 nanoparticles within agglomerates (Fig. 2d, e). This occurred after exposure to total electron fluences of as little as 20 $e^-/Å^2$ and could therefore bias this technique toward an over representation of smaller agglomerates or single particles no longer representative of the 'native' state. In addition, there was also a build-up of matter around the TiO_2 nanoparticles after exposure to the electron beam. EDX data showed this was C rich (Fig. S6 in SI), and therefore, we attribute it to hydrocarbon contamination during STEM acquisition. Potential opportunities to try and reduce some of these beam-induced artefacts could be to dilute the commercial sunscreen in alcohol rather than water. Alcohols such as ethanol can be used to act as scavengers in LC experiments [28], reacting with some of the radiolytic damage products in preference to the sample and thereby extending the life of the sample under the electron beam. However, care needs to be taken to ensure the dilution strategy does not alter the composition of the sunscreen, and analysis still remains a true representation of the product.

There was evidence of some oil/water separation, where oxygen-dense regions appeared in boundary to more carbon-rich areas (Fig. 3); this may be due to the immiscibility of oil in water and the need to dilute the sample before loading the k-kit. Whether these separate regions exist in the undiluted product however is not possible to say using this technique.

As a comparison and to address some of the limitations of the LC analysis, the sample was also characterised using cryo-analytical-S/TEM. The same diluted sample was used and both TiO_2 and ZnO nanoparticles were observed in the frozen sample, verifying that ZnO dissolution is prevented or at least

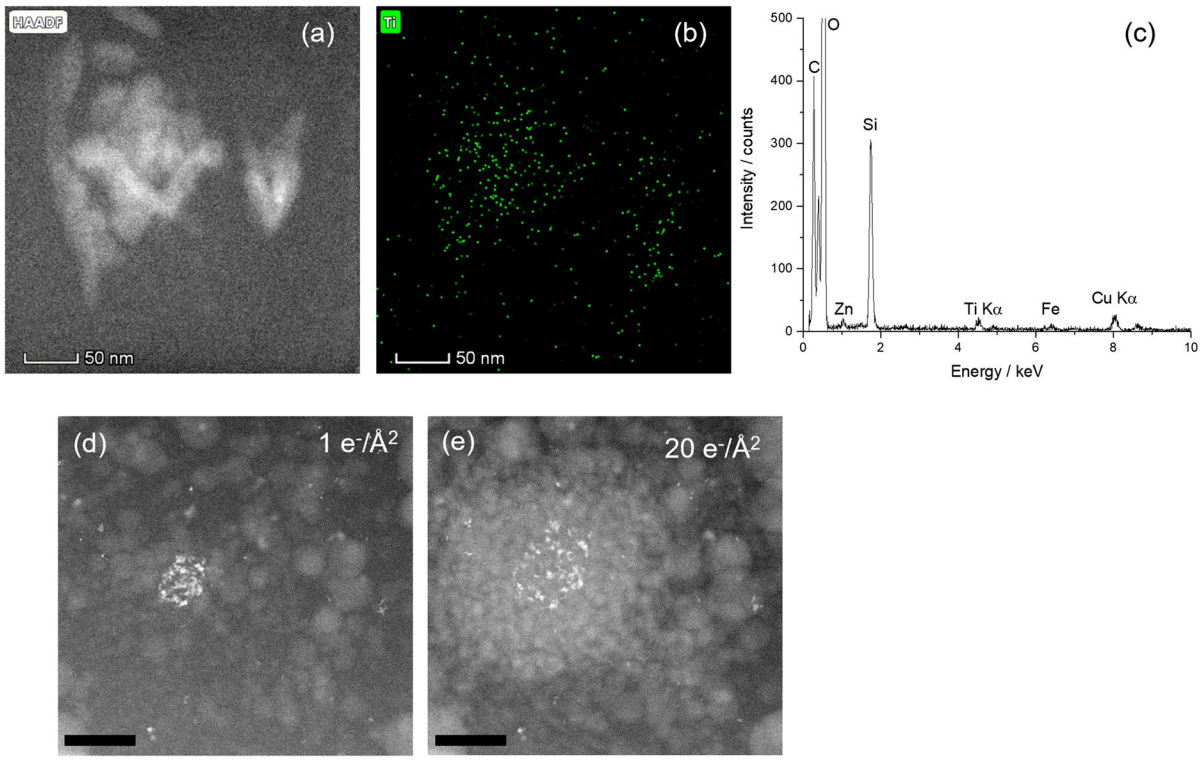

Fig. 2 **(a)** HAADF STEM image of TiO_2 nanoparticles in LCTEM showed TiO_2 nanoparticles primarily existed in small agglomerates. This was confirmed through EDX spectroscopy with **(b)** spatially resolving the position of Ti and the spectrum confirming signals for Ti and O. The strong Si signal is from the silicon nitride membrane windows in the k-kit. Electron beam induced movement of the TiO_2 nanoparticles was also observed and shown in **(d)** and **(e)**. The two images are of the same area with **(d)** the initial image and **(e)** after exposure to a further 20 $e^-/Å^2$. Clear movement of the TiO_2 particles was observed as the particles diffused away from the initial cluster. Scale bars in **(d)** and **(e)** are 500 nm

significantly delayed when using cryo techniques (Fig. 4). This then allowed obvious dispersion analysis of both nanoparticles, and it was observed that ZnO nanoparticles appeared to be present as small agglomerates as well as individual particles. In similarity to LCTEM, cryo-EM of the undiluted product was not possible due to the high viscosity of the sunscreen which resulted in ice that was too thick to image through.

Since neither cryo-TEM nor LCTEM allowed the commercial sunscreen to be imaged without dilution, cryo-SEM was used to do this. Additionally, this allowed two different samples to be imaged: the original sunscreen (i.e. no alteration to the as purchased commercial sunscreen) and the 'in-use' or sheared sunscreen which describes a sample of sunscreen rubbed between two glass slides for 10 min in order to mimic the process of applying sunscreen to skin. Independent of the sample preparation, i.e. sheared or unsheared, cryo-SEM imaging indicated the agglomerate size observed was the same within error between the two samples. This indicates the process of applying the sunscreen to skin does not alter the nanoparticle composition or dispersion of the original product. For both samples, nanoparticle agglomerates of a similar size to those observed in cryo-TEM and LCTEM were seen and EDX analysis indicated the presence of both ZnO and TiO_2 nanoparticles as expected (Fig. 5). However, larger agglomerates were also observed on the order of ~ 5 µm (Feret diameter) that had not been observed during cryo-TEM and LCTEM analysis of the diluted product. The average large agglomerate size for the unsheared and sheared samples was 4.89 ± 1.33 and 7.46 ± 3.30 µm, respectively. Backscattered electron images were advantageous in showing both the large and small

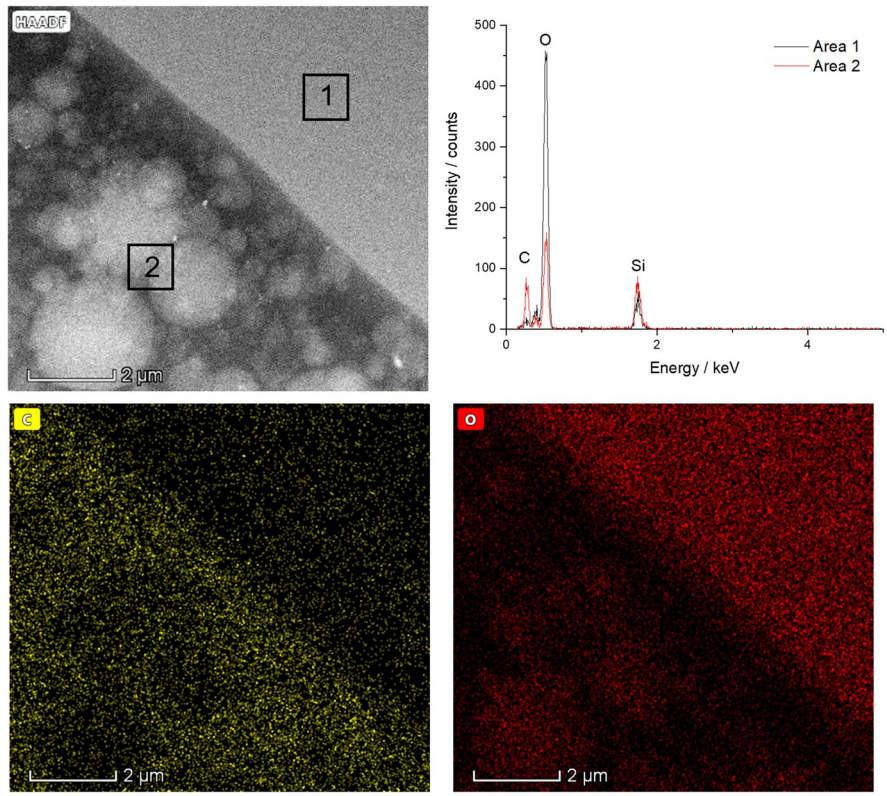

Fig. 3 STEM-EDX analysis of a diluted commercial sunscreen at 20 pA (0.12 e^{-}/Å.^{2}) using LCTEM. The HAADF STEM image shows separation of oil and water in the sunscreen with EDX spectra taken from both areas. Area 1 is O rich and area 2 C rich. This is confirmed in spatial mapping of C (yellow) and O (red)

agglomerates whilst only the larger agglomerates were visible in secondary electron images. Further advantages of BSE imaging is the ability to not only identify nanoparticle agglomerates but to use differences in contrast between nanoparticles to start to identify nanoparticle composition, based on prior knowledge. Heavier metal nanoparticles will appear brighter due to the larger nuclei deflecting more electrons back from the surface. In this case, therefore, we would presume the regions of brighter contrast relate to the ZnO nanoparticle agglomerates and the less bright regions to TiO_2. Using EDX, this can then be confirmed as was carried out here (Fig. 5). The discrepancy between the observation of larger agglomerates in cryo-SEM but not cryo-TEM or LCTEM could stem from a number of factors. For cryo-TEM, the blotting that precedes plunge freezing during sample preparation, could push out the larger agglomerates from the TEM grid or these larger agglomerates my just be too thick to image through. For LCTEM, the channel size of the k-kit used was 2000 nm; this would preclude agglomerates of a greater size from entering the cell. Furthermore, it was the undiluted sample that was imaged in cryo-SEM; this could then be due to some dilution artefact, although these larger agglomerates were not observed from the DLS experiments, though there must be a degree of caution here since typically DLS becomes less accurate at measuring sizes beyond 1 µm.

The presence of these larger agglomerates is likely to influence the performance of the product. Tyner et al. [3] have already shown that greater agglomeration can reduce the UV blocking capabilities, due to effectively reducing the surface area available to absorb and scatter UV light. It would be anticipated that more disperse nanoparticles throughout the sunscreen would result in a more efficient product. However, this is a commercial product with proven sun protection; this will come from the presence of smaller agglomerates alongside single particles that we have shown are also present within the product. Nevertheless, during product design using SEM techniques alongside S/TEM would be advantageous in order to prevent an inaccurate bias toward characterising only the smaller nanoparticle and agglomerate fractions.

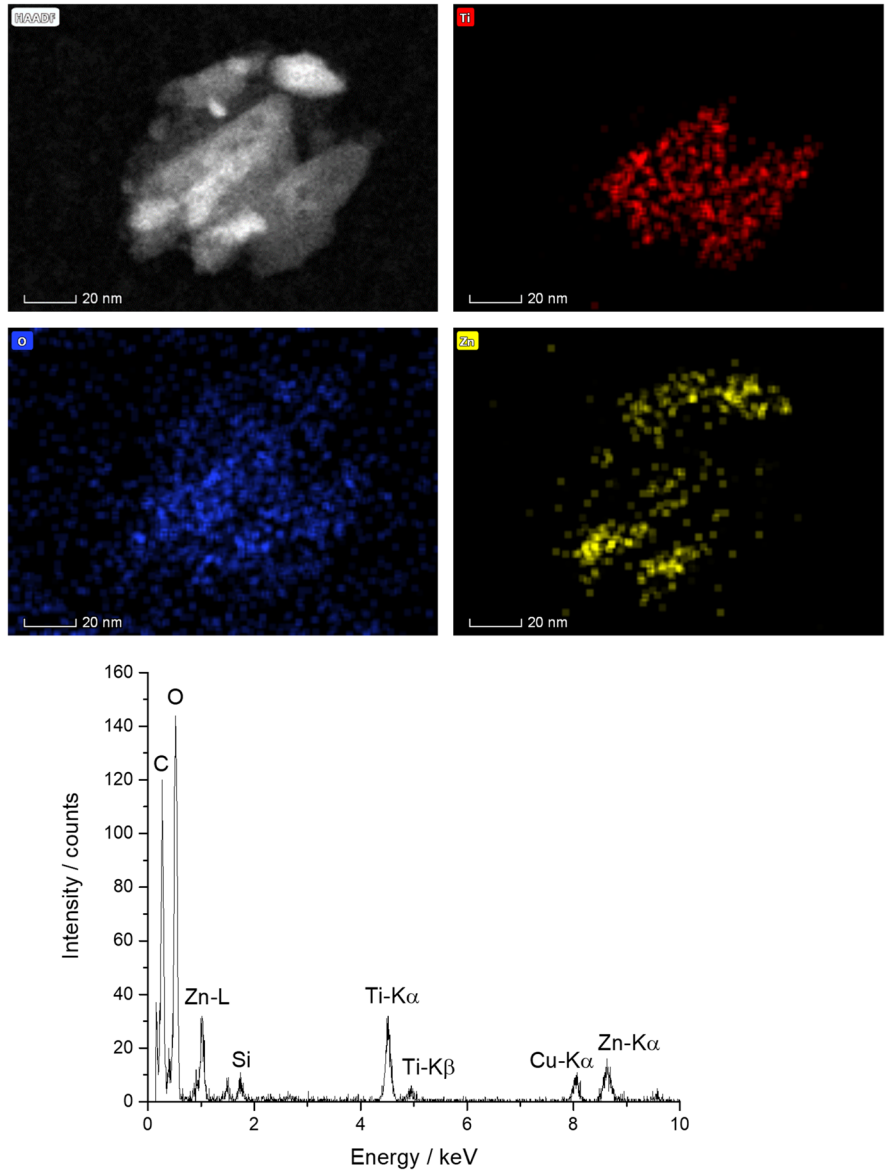

Fig. 4 Cryo-STEM-EDX of the diluted commercial sunscreen. Both TiO_2 and ZnO nanoparticles were identified and confirmed through spatial mapping of Ti (red), O (blue) and Zn (yellow)

It is common for TiO_2 or ZnO nanoparticles to have a coating when used in sunscreen in order to stabilise the colloidal dispersion. Here no technique indicated an obvious coating. However, typically coatings are polymeric with a high carbon content, such low weight atomic elements do not have strong contrast within EM and can also be prone to electron damage. Using bulk techniques however such as FT-IR cannot distinguish between the emulsion carrier and any coating present around the nanoparticles. Techniques to separate the nanoparticles from the product would therefore be necessary to fully confirm if any coating was around the nanoparticles.

Clearly, there is an argument that multiple techniques for nanoparticle dispersion characterisation are required in order to get a fuller picture of the range of agglomerates within a product to ensure applicability to its intended use (see SI Table S3 for overall summary of techniques). Additionally, the toxicological implications of nanoparticle-based products routinely used in cosmetic products remains a concern [29]. Thus far, we have suggested that beam-induced pH changes in LCTEM are detrimental, yet there is an argument they could be utilised for real-time toxicological studies. Specifically,

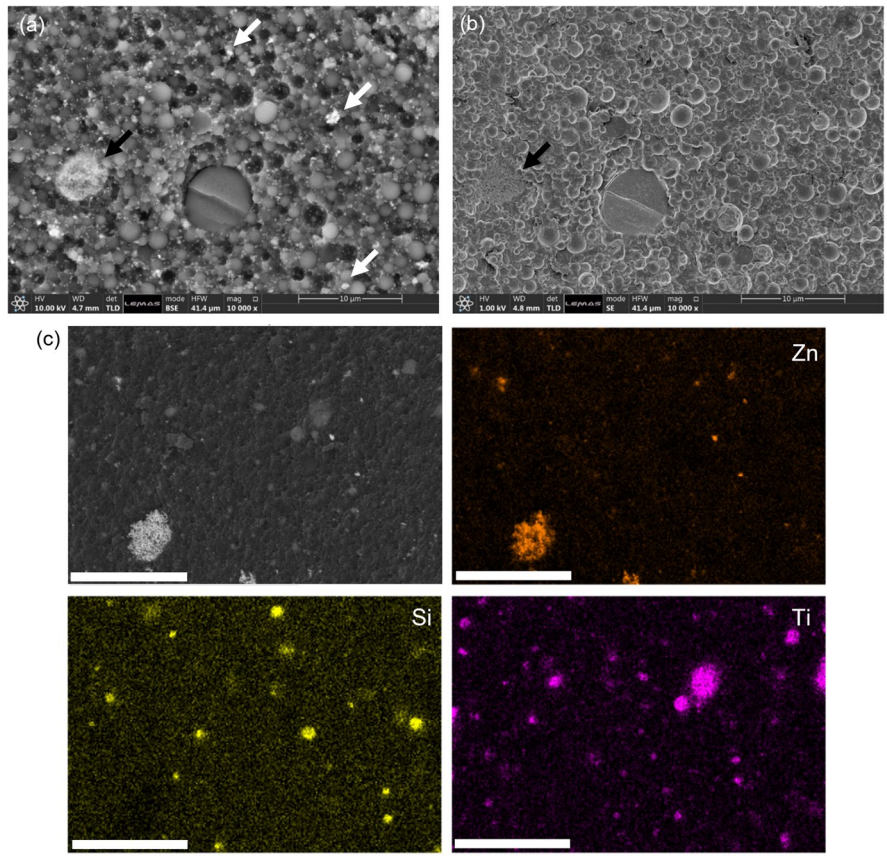

Fig. 5 **(a)** Cryo-SEM back scattered electron image taken using a 100 pA probe current showing both large (black arrow) and small (white arrow) nanoparticle agglomerates. The smaller agglomerates are not visible in the secondary electron image of the same area (**b**). (**c**) Cryo-SEM–EDX of the commercial sunscreens taken using a 15 kV accelerating voltage and 100 pA probe current. EDX mapping of Ti (pink) and Zn (orange) indicates the positions of the active nanoparticle agglomerates and Si (yellow) was also present as expected from the presence of dimethicone in the commercial sunscreen. Scale bar is 25 µm

endocytic cellular uptake of nanoparticles is seen as one of the main routes of entry into a cell. This process involves nanoparticles entering endosome and lysosomes, both low pH environments. Research has been conducted into the behaviour of nanoparticles in these environments [30], with the dissolution of inorganic metal nanoparticles known to cause the production of toxic reactive oxygen species [31]. It may be possible that in mimicking these common acidic environments real-time nanotoxicology analysis could be carried out using LCTEM.

Ultimately, it is our recommendation that where possible a combination of techniques for full characterisation of nanoparticle dispersions are carried out. We have demonstrated that there are limitations and advantages of both cryo-EM and LCTEM, where beam interactions that become problematic when using LCTEM can be delayed by analysis of a frozen sample. Nonetheless, LCTEM is arguably the truest form of analysis with no sample preparation required and could be used for important in situ toxicological studies. As a minimum, multi-nanoparticle suspensions should be characterised by using at least one in situ EM technique alongside bulk analysis in order to better distinguish signals from individual particles. Such utilisation of in situ analytical EM will allow more effective and safer commercial products to be formulated.

Funding The electron microscopes used in this work were funded by the Engineering and Physical Sciences Research Council (EPSRC), UK under grants EP/P00122X/1 (Helios FIB-SEM) and EP/M028143/1 (FEI Titan Themis). Funding is also provided by the EPSRC via Programme Grant No. EP/R018820/1 which funds the "Crystallisation in the Real World" Consortium, and further financial support is provided by the EPSRC to NH in the form of a New Investigator Award (EP/R043388/1).

Declarations

Conflict of interest The authors declare no competing interests.

References

1. Cole C, Shyr T, Ou-Yang H (2016) Metal oxide sunscreens protect skin by absorption, not by reflection or scattering. Photodermatol Photoimmunol Photomed 32(1):5–10
2. Popov AP et al (2005) TiO2nanoparticles as an effective UV-B radiation skin-protective compound in sunscreens. J Phys D Appl Phys 38(15):2564–2570
3. Tyner KM et al (2011) The state of nano-sized titanium dioxide (TiO2) may affect sunscreen performance. Int J Cosmet Sci 33(3):234–244
4. Barnard AS (2010) One-to-one comparison of sunscreen efficacy, aesthetics and potential nanotoxicity. Nat Nanotechnol 5(4):271–274
5. Lewicka ZA et al (2011) The structure, composition, and dimensions of TiO2 and ZnO nanomaterials in commercial sunscreens. J Nanopart Res 13(9):3607
6. Braydich-Stolle LK et al (2009) Crystal structure mediates mode of cell death in TiO2 nanotoxicity. J Nanopart Res 11(6):1361–1374
7. Davey S (2010) Sunscreen size studies. Nat Chem
8. Ilett M, Wills J, Rees P, Sharma S, Micklethwaite S, Brown A, Brydson R, Hondow N (2020) Application of automated electron microscopy imaging and machine learning to characterise and quantify nanoparticle dispersion in aqueous media. J Microsc 279:177–184. https://doi.org/10.1111/jmi.12853
9. Ispas C et al (2009) Toxicity and developmental defects of different sizes and shape nickel nanoparticles in zebrafish. Environ Sci Technol 43(16):6349–6356
10. Favi PM et al (2015) Shape and surface effects on the cytotoxicity of nanoparticles: Gold nanospheres versus gold nanostars. J Biomed Mater Res A 103(11):3449–3462
11. Deegan RD et al (1997) Capillary flow as the cause of ring stains from dried liquid drops. Nature 389(6653):827–829
12. Dieckmann Y et al (2009) Particle size distribution measurements of manganese-doped ZnS nanoparticles. Anal Chem 81(10):3889–3895
13. Ilett M et al (2019) Cryo-analytical STEM of frozen, aqueous dispersions of nanoparticles. Micron 120:35–42
14. Woehl TJ et al (2013) Experimental procedures to mitigate electron beam induced artifacts during in situ fluid imaging of nanomaterials. Ultramicroscopy 127:53–63
15. Schneider NM et al (2014) Electron–water interactions and implications for liquid cell electron microscopy. J Phys Chem C 118(38):22373–22382
16. Elliot AJ, Bartels DM (2009) The reaction set, rate constants and g-values for the simulation of the radiolysis of light water over the range 20 deg to 350 deg C based on information available in 2008. Atomic Energy of Canada Ltd; Report number AECL-153–127160–450–001: Canada, p 162
17. Sterniczuk M, Bartels DM (2016) Source of molecular hydrogen in high-temperature water radiolysis. J Phys Chem A 120(2):200–209
18. Speedy RJ, Angell CA (1976) Isothermal compressibility of supercooled water and evidence for a thermodynamic singularity at −45°C. J Chem Phys 65(3):851–858
19. Ilett M, Freeman HM, Aslam Z, Galloway JM, Klebl DP, Muench SP, McPherson IJ, Cespedes O, Kim Y-Y, Meldrum FC, Yeandel SR, Freeman CL, Harding JH, Brydson RMD (2022) Evaluation of correlated studies using liquid cell and cryo-transmission electron microscopy: hydration of calcium sulphate and the phase transformation pathways of bassanite to gypsum. J Microsc 288:155–168. https://doi.org/10.1111/jmi.13102
20. Liu K-L et al (2008) Novel microchip for in situTEM imaging of living organisms and bio-reactions in aqueous conditions. Lab Chip 8(11):1915–1921
21. Lu PJ et al (2015) Characterizing titanium dioxide and zinc oxide nanoparticles in sunscreen spray. Int J Cosmet Sci 37(6):620–626
22. Trang NTT, Chang J, Chen W-A, Chen C-C, Chen, H-M, Chang C-C, Fong T-H (2020) A novel microchip technique for quickly identifying nanogranules in an aqueous solution by transmission electron microscopy: imaging of platelet granules. Appl Sci 10:4946. https://doi.org/10.3390/app10144946
23. Tai L-A et al (2012) Quantitative characterization of nanoparticles in blood by transmission electron microscopy with a window-type microchip nanopipet. Anal Chem 84(15):6312–6316
24. BioMa-Tek. MA-tek's enabling solution for liquid analysis by TEM; https://www.bioma-tek.com/bioma-tek/en/goods.php?act=view&no=61. [cited 2023 Jan]
25. Le Caër S (2011) Water radiolysis: influence of oxide surfaces on H2 production under ionizing radiation. Water 3(1):235
26. Bian S-W et al (2011) Aggregation and dissolution of 4 nm ZnO nanoparticles in aqueous environments: influence of pH, ionic strength, size, and adsorption of humic acid. Langmuir 27(10):6059–6068
27. Mu Q et al (2014) Systematic investigation of the physicochemical factors that contribute to the toxicity of ZnO nanoparticles. Chem Res Toxicol 27(4):558–567
28. Woehl TJ, Abellan P (2017) Defining the radiation chemistry during liquid cell electron microscopy to enable visualization of nanomaterial growth and degradation dynamics. J Microsc 265(2):135–147
29. Ruszkiewicz JA et al (2017) Neurotoxic effect of active ingredients in sunscreen products, a contemporary review. Toxicol Rep 4:245–259
30. Soenen SJH et al (2010) Intracellular nanoparticle coating stability determines nanoparticle diagnostics efficacy and cell functionality. Small 6(19):2136–2145
31. Liu J et al (2017) Zinc oxide nanoparticles induce toxic responses in human neuroblastoma SHSY5Y cells in a size-dependent manner. Int J Nanomed 12:8085–8099